Aggregation of Fibers by Waves

Gautier Verhille and Patrice Le Gal

Abstract Sea balls also called aegagropila, can be found on Mediterranean beaches. They are made of *Posidonia* fibers, which aggregate on the seabed due to the sea motions. To understand the mechanism of aggregation and compaction of these structures, we have performed a laboratory investigation on the dynamics of aggregation of fibers by surface gravity waves generated in a water tank. Amazingly, depending on the flexibility of the fibers, two different sites of aggregation are observed. Following our experiments, we propose an analytical derivation of the clustering of particles by the Stokes drift. This theoretical calculation is quite general and emphasizes the respective roles of the Stokes number and the density of the particles; it also underlines the importance of the fiber flexibility in their drift and explains our experimental observations.

Keywords Fiber aggregation · Fiber dynamics in flow · Stokes drift

1 Introduction

Aegagropila are sea balls composed of *Posidonia* fibers, which can be found along the Mediterranean beaches. *Posidonia* are aquatic plants that fade in autumn. Their roots then release on the seabed a large quantity of fibers that will get caught by the sea water flows and waves. After a certain time (still unknown), clusters of entangled fibers are deposited on the beaches in the form of compact balls. These structures have a large size dispersion (a few millimeters for the smaller ones to about ten centimeters for the larger ones). Figure 1a presents a photograph of these sea balls constituted by one to two centimeter long fibers having a diameter around 100 μm. A statistical study of the size and mass of aegagropila shows that these distributions obey a lognormal law,

G. Verhille (✉) · P. Le Gal
Aix-Marseille Univ, CNRS, Centrale Marseille, IRPHE, Technopôle de Château Gombert, 49 Rue F. Joliot Curie, BP 146, 13384 Marseille Cedex 13, France
e-mail: verhille@irphe.univ-mrs.fr

P. Le Gal
e-mail: legal@irphe.univ-mrs.fr

N. Abcha et al. (eds.), *Nonlinear Waves and Pattern Dynamics*,
https://doi.org/10.1007/978-3-319-78193-8_8

Fig. 1 **a** Photographs of *Posidonia* aegagropila (Plage du Prophète, Marseille). **b** Close up of the extremities of a marine rope piece, where some fibers have been agglomerated on the nylon fiber bundles. **c** Two aegagropila that have aggregated on a textile thread

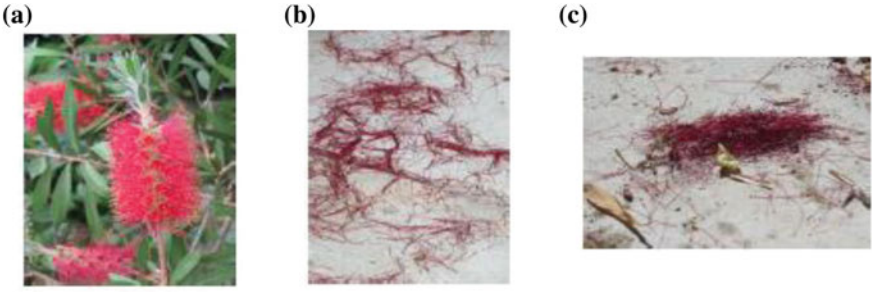

Fig. 2 **a** Photograph of a bottlebrush flower (Marseille). **b** Bottlebrush flower stamens fallen on the floor in the course of aggregation under the action of a turbulent wind. **c** An aggregate of bottle brush flower fibers

which is compatible with an aggregation of fibers trapped randomly by the forming balls [1]. Some of these fiber aggregates can also be encountered around *Posidonia* rhizome fragments or even foreign bodies as it is the case in Figs. 1b, c, where the fibers have been trapped on the extremities of a marine rope piece or along a textile thread. These examples show if the aggregation process does not need any nucleus, some of the sea balls possess synthetic or natural nuclei that may help their formation.

More generally, natural fibers have the tendency to agglomerate to form bundles or balls when agitated by fluid turbulent motions. Figure 2 presents an example of aggregation of fibers in air: under the action of wind, bottlebrush (*Callistemon*) flower stamens whose length is around 3 cm for a diameter about 300 μm aggregate when they fall on the floor. Figure 3 gives another example of natural fiber accretion by the sea, but this time of living seaweeds. Contrary to the short fibers of *Posidonia* or bottlebrush flower fiber aggregates, in the case of these long seaweeds, fiber self-entanglements are certainly at the origin of the bundles that can be seen along the shore.

These different structures pose several questions ranging from their formation (physical mechanisms, duration of the aggregation process, etc.) to the understanding of the observed size distributions. In the absence of in situ measurements, we propose to study in the laboratory, the dynamics of formation of fiber clusters in a simple flow generated by the periodic excitation of surface waves in a tank. Then, we will

Fig. 3 Photographs of seaweed aggregates along the Pacific seashore (Gator beach, San Diego, California). The length of the seaweeds, between ½ and 1 m, enhances self-entanglements that sustain the aggregates (pen length ~15 cm)

propose a nonlinear model that explains the observed transport of the fibers by a flow.

2 Experimental Observation of Fiber Aggregation in a Flow

2.1 Experimental Device

In order to stay close to the back and forth movement that exists at the bottom of the sea, we choose to study the dynamics of fibers in a flow induced by the oscillation of a plate in a basin of length L = 80 cm (along the x direction). The basin is 28 cm wide (y direction) and 40 cm deep in the vertical z direction. When oscillating at angular frequency ω, the plate drives a stationary wave in a $h = 10$ cm deep layer of water. The two-dimensional flow field can then be approximated by a periodic potential ϕ:

$$\phi = U_0 \cos(kx) \cosh((z + h)/\lambda) \sin(\omega t), \tag{1}$$

where $k = 2\pi/\lambda$ is the wave number of the surface gravity wave and λ its wavelength. The resonance frequency of the basin is close to 0.8 Hz. In order to test the influence of fiber stiffness on the formation of aggregates, we used two types of fiber material: nylon and cotton. The length of the threads is around 5 cm and the diameter of the cotton threads is 150 and 400 μm for the nylon threads. Therefore, the aspect ratio of the fibers that we use in the experiment is between 100 and 300, i.e., in the same order of magnitude of the aspect ratio of the *Posidonia* fibers found in natural aegagropila (50–100). The cotton fibers are very flexible and can be easily deformed in the flow while the nylon fibers are rigid and do not deform. In both cases, the density of the fiber material is greater than the one of the fluid and since the flow velocities are relatively small, all the dynamics occurs on the smooth bottom of the basin. Finally, only a unique concentration of threads (500 threads in total) will be considered here.

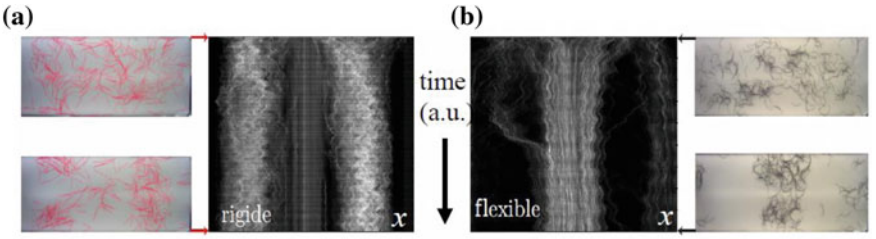

Fig. 4 Comparison of the dynamics of rigid fibers (**a**) and flexible fibers (**b**) in the experiments. Above and below on each side, are the initial and final conditions of the experiment, respectively. In the center, the space-time diagrams visualize the dynamics of fiber agglomeration toward the quarter and three-quarters of the basin for the rigid nylon fibers and toward the center for the flexible cotton fibers

2.2 Localization of the Fiber Aggregates

Consider first, a forcing frequency below the resonance frequency. The amplitude of the surface wave at the free surface is around 1 cm with a wavelength of 0.8 m. At initial time, the threads are arranged randomly (in position and orientation) on the bottom of the basin. After several hours, once the equilibrium is reached, we see in Fig. 4 that the threads have migrated toward some particular locations in the basin: the rigid nylon fibers (on the left of Fig. 4) are mainly located at a quarter and three-quarters of the tank length, whereas the flexible cotton fibers (on the right of Fig. 4) go mainly to the center of the basin. It is found that in both cases, at least during the 5–10 h of the experimental run duration, the clusters are not very tight and compact.

In order to understand the localization of these clusters, we propose in the following a one-dimensional model since Fig. 4 shows that the system is almost invariant over the width of the tank (this is expected because of the symmetries of the forcing and because of the random initial conditions). Because each fiber is first rapidly oriented in the flow before it drifts, it is fully justified to model it by a point particle moving in a velocity field as described by the potential flow given by Eq. (1). By neglecting the history terms (Basset terms) and the interactions between particles, the equation of evolution of the velocity of a spherical particle v_p is simply [2]:

$$dv_p/dt = \alpha Du/Dt + \left(u - v_p\right)/St, \tag{2}$$

where d/dt and D/Dt represent the Lagrangian derivative when following a solid particle and the Lagrangian derivative when following a fluid particle, respectively. The density coefficient α is equal to $3\rho_f/(2\rho_f + \rho_p)$, where ρ_f and ρ_p are the fluid and the solid particle density. When α is less than unity the particles sink at the bottom of the fluid layer contrary to the cases when α is larger than 1, where particles float on the fluid surface. The Stokes number characterizes the relative importance of inertia

to viscous effects. For instance, for a spherical particle of radius a, immersed in a fluid of kinetic viscosity ν_f, the Stokes number reads:

$$St = 2a^2\omega/3\nu_f\alpha$$

In Eq. (2), all magnitudes are made dimensionless using the wavelength λ for the lengths, the inverse of the angular frequency $1/\omega$ for the time and U_0 for the velocities. Thus, the forcing velocity field at a fixed depth z near the bottom of the tank is simply $u = \sin(x)\sin(t)$. Using these quantities, and the fact that the flow is essentially one-dimensional at the bottom of the basin along its length, the Lagrangian total derivatives can be cast under the form:

$$d/dt = \partial_t + \varepsilon v_p \partial_x \quad \text{and} \quad D/Dt = \partial_t + \varepsilon u \partial_x,$$

where ε is equal to $U_0/\omega\lambda$. Using the orders of magnitude of the experimental parameters (observed velocity $U_0 \sim 1$ cms^{-1}, frequency $\omega \sim 1$ Hz and $\lambda \sim 1$ m), we can estimate that the order of magnitude of ε is around 10^{-2}. Therefore, ε can be considered as a small parameter and this will allow studying the solutions of the particle transport Eq. (2) and their stability by making a perturbative development in power of ε:

$$v_p = v_p^0 + \varepsilon v_p^1 + \varepsilon^2 v_p^2 + \ldots$$

At order 0 in ε, introducing the shape of the fluid velocity field in Eq. (2), leads to the determination of v_p^0 with the condition that $v_p = 0$ at initial time:

$$v_p^0 = (A\sin t + B(\cos t - e^{-t/St}))\sin x, \tag{3}$$

where the analytical expressions of the coefficients A and B are:

$$A = (1 + \alpha St^2)/(1 + St^2),\ B = St(\alpha - 1)/(1 + St^2)$$

The two first terms in (3) represent the stationary oscillatory response of the particle to the oscillatory forcing of the flow. This stationary oscillation will be reached after a transient represented by the third term, which is parametrized by the Stokes number St. We can see on formula (3) that the fixed points, i.e., the positions in the basin, where the particles will always stay at the same place are $x_e = 0$ or $x_e = \pm\pi$, thus at the center and near the sidewalls of the tank. At this order, we can also see that after the transient, the time-averaged velocity of any particle will be zero: $\langle v_p^0 \rangle = 0$. The drift of the particles, which is here at the origin of aggregation in our experiment does not appear at this zero order in ε and will only be recovered when taking into account the nonlinearity of Eq. (2) as expected for a Stokes drift. The integration of Eq. (2) at first order in ε, leads to the analytical expression of v_p^1:

$$v_p^1 = \sin 2x[St(\alpha - A^2 - B^2)/2 + C\cos 2t + D\sin 2t$$

$$+ (B^2 \sin t + 2AB \cos t + \delta)\, e^{-t/St} + e^{-2t/St} B^2 St/2)]/2$$

with the following constants:

$$C = [4ABSt^2 + St(A^2 - B^2 - \alpha^2)]/2(1 + 4St^2),$$
$$D = (A^2 - \alpha - B^2 St^2 - ABSt)/2(1 + 4St^2)$$

and δ, a constant of integration that allows to set $v_p = 0$ at initial time.

The transients having disappeared, the mean velocity in time $\langle v_p^1 \rangle$ is non zero now because of the first term in the expression of v_p^1. This nonzero drift velocity $Vs = \langle v_p^1 \rangle$ gives rise to what is classically called the Stokes drift of the particles. The physical meaning of this drift comes from the fact that the oscillating flow is nonhomogeneous as its amplitude varies along the x axis of the tank. Therefore, after one period of oscillation, a particle never comes back exactly at the same position in space and as a consequence slowly drifts in time. This phenomenon should be similar to the drift of sand grains by steady streaming that forms seabed ripples under shallow water waves [3, 4]. In our case, this drift velocity can be analytically calculated:

$$Vs = \sin 2x(1 - \alpha)(\alpha St^2 - 1)/4\left(1 + St^2\right)^2$$

So, depending on the sign of Vs, the equilibrium positions $x_e = 0$ or $x_e = \pm \pi$ can be either stable or unstable. The calculation of the sign of Vs leads to the diagram presented in Fig. 5 that presents the repulsive or attractive characteristics of the positions x_e as a function of St and α. When $\alpha < 1$ (particles denser than the fluid), the aggregates are located in $x_e = 0$ or $x_e = \pm \pi$, that is at the center and the sidewall of the container. This case is stable for $St^2 < 1/\alpha$ (white area on Fig. 5) and corresponds to the situation, where the friction force $(u\text{-}v_p)/St$ acting on the particle is greater than the pressure force. In the opposite case, the drift of the particle is dominated by inertia effects (gray areas). Note that this criterion is exactly the same as the one found by Xu and Nadim in the case of the drift of particles under the action of the Coriolis force in a librating flow [5].

The numerical integration of the particle dynamics Eq. (2) confirms the previous stability analysis result. As an initial condition, we consider 128 particles homogeneously distributed on a line between $-\pi$ and π. Integration in time of Eq. (2) reproduces the two cases that we have discovered analytically. In the first case, where the equilibrium positions are stable, we observe that the particles slowly drift and merge at the expected locations $x_e = 0$ or $x_e = \pm \pi$. The numerical space-time plot of Fig. 5a illustrates this case. In the other case, when the drift velocity expels the particles from the equilibrium positions x_e, we found that the nonlinear solution converges toward limit cycles, where the particles oscillate indefinitely around $x_c = \pm \pi/2$. Figure 5b illustrates this computation.

The comparison of the space-time diagrams of Figs. 4 and 6 shows that the dynamics of the rigid nylon fibers correspond to case, where $x_e = 0$ or $x_e = \pm \pi$ are repulsive, whereas the dynamics of the flexible (cotton) fibers correspond to that of the case,

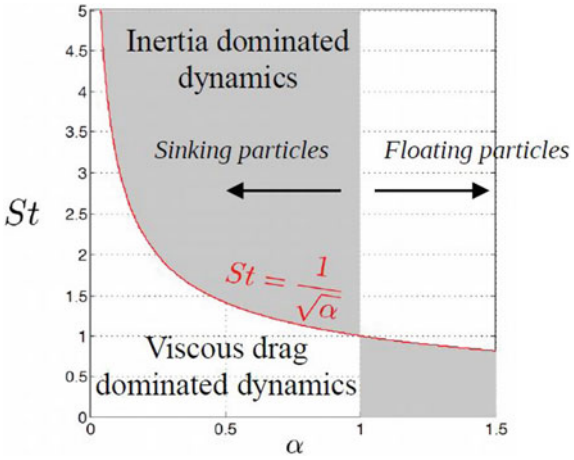

Fig. 5 Stability diagram of the equilibrium positions x_e as function of the Stokes number *St* and the density parameter α. The gray areas correspond to cases, where x_e are unstable and the white areas to cases, where x_e are stable

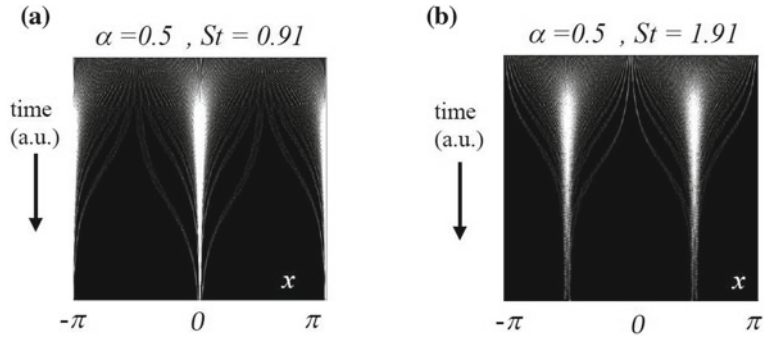

Fig. 6 Numerical simulations of the drift of 128 particles (without interaction) in a periodic flow U_0 sin(*x*) sin(*t*). Space-time diagram of the dynamics: **a** attraction of the particles in locations $x_e = 0$ or $x_e = \pm \pi$; **b** repulsion of the particles from locations $x_e = 0$ *or* $x_e = \pm \pi$ and attraction by limit cycles around $x_c = \pm \pi/2$

where $x_e = 0$ or $x_e = \pm \pi$ are attractive. Since the geometry and density of the two types of fibers are very close ($\rho_p \sim 1.2$ kg m^{-3} for nylon and $\rho_p \sim 1.4$ kg m^{-3} for cotton), it seems that the difference in behavior is more likely associated with the stiffness of the two different fibers. Indeed, we think that flexible fibers are less sensitive to inertia effects as they can deform under the action of pressure forces. Therefore, it is logical to observe the drift of the flexible cotton fibers toward x_e. On the contrary, the rigid, nondeformable nylon fibers are more sensitive to pressure, and thus drift away from x_e as expected from the model.

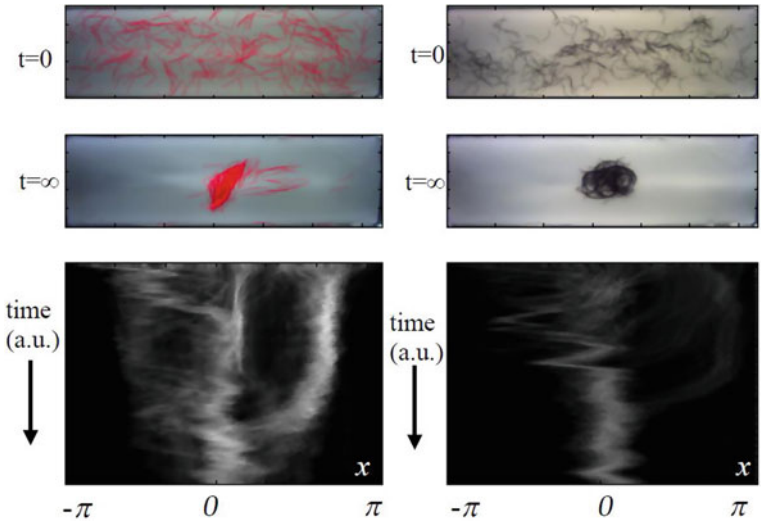

Fig. 7 Pictures of the initial and final states in the case of compaction of rigid nylon fibers (left) and flexible cotton fibers (right). Corresponding spatiotemporal diagrams revealing the compaction dynamics

Let us consider now a forcing with a frequency ω around the resonance frequency resulting in a wave having an amplitude larger than in the previous experiments. Moreover, a transverse mode of oscillation appears also in the tank. We see in Fig. 7 that relatively compact clusters are formed now and that whatever the nature of the fibers, these balls stand in the center of the basin after the experiments have run several hours. The associated space-time diagrams of Fig. 7 show, however that, in the case of the rigid nylon wires, the aggregation occurs initially (and as before) at $x_c = \pm\, \pi/2$ before the cluster drifts to the equilibrium location $x_e = 0$. This original phenomenon can be understood using our model as presented earlier. A time $t = 0$, the rigid nylon fibers are expelled from the fixed points toward attractors located at $x_c = \pm\, \pi/2$. The forcing being sufficiently strong this time and three-dimensional because of the presence of basin transverse mode, the fibers will form a deformable cluster of fibers, which in consequence increases the influence of the viscous force and reduces the effects of pressure. After a certain time, the cluster behaves as a deformable particle and migrates as a whole to the fixed equilibrium points as expected for flexible particles by our model and as observed in the experiments.

Finally, to follow the compaction rate in time, we have defined the ratio β of the projected areas occupied by the fibers on the bottom of the tank (the black pixels on the video images) to the total horizontal section of the basin. β is a function of time and the ratio of β by the initial β_0 represents the compaction rate of the system. The temporal evolution of the averages on ten independent realizations of the ratio β/β_0 is represented in Fig. 8 for both cotton and nylon fibers. As can be seen, clear power laws are visible for both rigid fibers and flexible fibers clustering. Power laws fit of

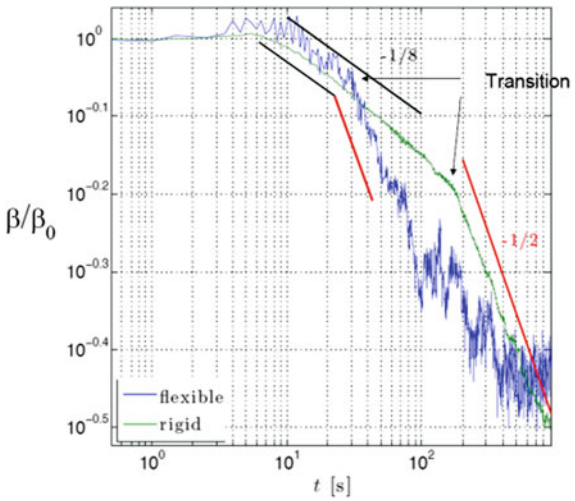

Fig. 8 Evolution of the compaction rate β/β_0 as a function of time. An average of 10 independent realizations have been performed. Power laws are clearly visible in both cases with a transition in the exponent values

the experimental curves give an exponent close to $-1/8$ at the beginning of the run (up to 10 s for the flexible fibers, and up to 100 s for the rigid ones). A transition then occurs and a regime with power laws with an exponent equal to $-1/2$ takes place in both cases. We suspect that the appearance of fiber interactions to be at the origin of these power laws that escape our modeling.

3 Conclusion

Inspired by the observation of natural aggregates formed by the motions of air or sea water, our studies on the dynamics of formation of fiber aggregates show that the Stokes drift is at the origin of the movement of the fibers and finally of their clustering in our set-up. The location of the clusters in the experiment is understood by the study of the stability of the fixed points of the particle dynamics equation when forced by a simple periodic (in space and time) fluid velocity field. A criterion based on the relative magnitude of the pressure effects compared to the viscous drag is deduced from a simple one-dimensional point particle model. This criterion based on the zeroing of the Stokes drift is quite general and may be useful to understand and even promote particle segregation. Our experiments, using flexible or rigid fibers confirmed the predicted attractive (where the aggregates form) or repulsive locations. This model even leads to the interpretation of the difference in behavior between rigid and flexible fibers. Finally, we observe that the aggregation process obeys temporal power laws that escape our modeling and are probably related to fiber interactions.

Acknowledgements This work has received funding from the Labex MEC Project (No. ANR-10-LABX-0092) and from Excellence Initiative of Aix-Marseille University—A*MIDEX, a French "Investissements d'Avenir" programme.

References

1. Verhille G., Moulinet S., Vandenberghe N., Adda-Bedia M. and Le Gal P. (2017) Structure and Mechanics of Aegagropilae Fiber Network. PNAS x: pp-pp.
2. Maxey M.R. and Riley J.J. (1983) Equation of motion for a small rigid sphere in a non uniform flow. Phys. Fluids 26: 883–889.
3. Blondeaux P. (1990) Sand ripples under sea waves. Part 1. Ripple formation. J. Fluid Mech. 218: 1–17.
4. Larrieu E, Hinch J. and Charru F (2009) Lagrangian drift near a wavy boundary in a viscous oscillating flow. J. Fluid Mech. 630: 391–411.
5. Xu S. and Nadim A. (2016) Oscillatory counter-centrifugation. Physics of Fluids 28 (2), 021302.